16th ICAAR LISBOA 2020-2022

16th International Conference on
Alkali-Aggregate Reaction in Concrete
Lisboa | LNEC | Portugal | 31 May - 2 June 2022

http://icaar2020-2022.lnec.pt

Modelling the behavior of ASR affected structures using homogenized reinforced concrete finite elements

Daniela Vo[(1)], Pierre Morenon[(1)], Stéphane Multon[(1)], Alain Sellier [(1)], Etienne Grimal[(2)], Benoit Masson[(3)], Anass Cherki El Idrissi[(4)], Philippe Kolmayer[(2)]

(1) LMDC, Université de Toulouse, UPS, INSA, 135, avenue de Rangueil, F-31 077 Toulouse Cedex 04, France

(2) Electricité de France, Centre d'Ingénierie Hydraulique, EDF-CIH Technolac, 73373 Le Bourget du Lac, Cedex, France

(3) Electricité de France, Division Ingénierie Nucléaire, EDF-DIPNN- 19 rue Pierre Bourdeix 69007 Lyon, France

(4) Electricité de France, Recherche et Développement, EDF Lab Paris Saclay, 7 boulevard Gaspard Monge, 91120 Palaiseau, France

Abstract

Alkali-Silica Reaction (ASR) is a serious disorder which can cause important degradations in concrete structures. Massive constructions can be subjected to this kind of disorder and their mechanical evolution over time must be known to ensure their safety. Numerical modelling is necessary to predict such behaviour. Some massive structures have dense reinforcement frames. It can imply an important modelling time particularly to obtain appropriate mesh. In this paper, a model is used to obtain homogenized reinforced concrete. With this approach, it is not necessary to explicitly mesh the reinforced bars in the concrete. It highly decreases both the meshing and the computation times.

The main subject of this study is the validation of the response of this model in an ASR context. Two reinforced concrete beams drawn from an experimental program of the literature are modelled. The structures responses are evaluated during the aging of concrete when the beams are progressively affected by the ASR and during the failure phase when the beams are subjected to a four-point bending test until failure. After the description of the main features of the model, the comparison between experimental and numerical results is presented. Two main model's features are needed to faithfully reproduce the experimental behaviour: the cracking anisotropy and the chemical prestress induced by the swelling restrained by the reinforcement.

Keywords: *anisotropy; chemical prestress; cracking; finite elements; modelling; reinforced concrete*

1. INTRODUCTION

Alkali-Silica Reaction (ASR) is an endogenous concrete swelling reaction. It takes place at the material scale thus altering the behaviour at structural scale. It is induced by chemical reactions between amorphous or low crystallised siliceous phases contained by reactive aggregates and alkalis present in the interstitial solution. This reaction produces swelling ASR-gels which can spread in and out of their initial reactive sites leading to concrete cracking. Consequently, such swelling in a concrete matrix already hardened can significantly reduce its durability by cracks and loss of mechanical strength. In certain environmental conditions, this kind of reactions can happen over several decades.

This pathology has been worldwide observed, notably in massive construction like bridges, dams or even in nuclear power plants. So, the evaluation of the behaviour of such damaged structures is needed to ensure their safety. To answer this request, number of researchers have developed models to predict the evolution of ASR-affected structures. Moreover, the damaged structures can be strongly reinforced. The modelling of these reinforcement frames induces some complexities. First, the presence of reinforcement in expansive concrete can lead to numerical problems induced by the incompatibility of deformations, mainly in the interface zone between swelling concrete, with great positive deformations, and steel restraining these deformations. Such mechanical conditions lead to stress-concentration and can cause unrealistic response with too important damage in the steel-concrete interface zone. The final consequence of such incompatibility can be the loss of bond between concrete and reinforcement.

Moreover, explicitly meshing all the steel bars of some structures can be particularly complex and time-consuming.

To avoid such numerical difficulty, a homogenized reinforced concrete model [1] [2] [3] is used in this study. With such approach, reinforcement does not need to be meshed explicitly. Steel contributions are reproduced by homogenized constitutive law. In reinforced part of the structure, each element represents a reinforced concrete material. Damage law and plastic criterion are applied to obtain a realistic representation of the damaged concrete. They are used to evaluate the plastic deformation due to ASR-expansion and consequently the induced cracking. By different criteria, the model presented in this work differentiates the localised cracking induced by structural loading and diffuse cracking induced by ASR-swelling at microscopic scale [4].

The aim of this study was to implement the model of homogenized reinforced concrete in a finite element code and to validate it in an ASR-context on a laboratory structure during its aging and up to its failure. The validation is based on tests presented by Ohno et al [5]. After an aging-period, a reactive and a non-reactive beam were submitted to a four-point bending test until failure. Two aging periods were studied, one for seventeen months and the other for forty-five months. The effect of chemical prestress due to ASR expansion induced some modifications compared to usual flexural behaviour for the reactive beam, like a different evolution of the flexural stiffness and a modification of the final crack pattern. To analyse the effect of ASR on the structural behaviour and validate the approach proposed in this paper, the model of homogenized reinforced concrete is used to evaluate the load-displacement curves and ultimate crack pattern and compared with the experimental results.

2. MODEL FORMULATION

2.1 Rheological model of homogenized reinforced concrete

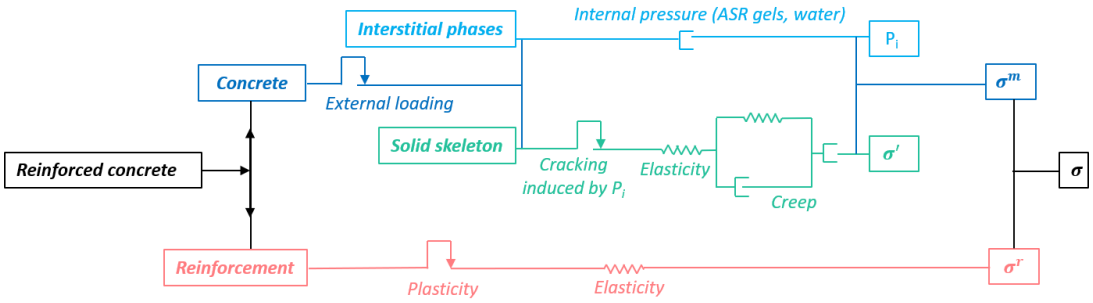

Figure 2.1: Rheological scheme of homogenized reinforced concrete

The model used in this study is based on a homogenized mechanical constitutive law. The structural response of reinforced concrete is averaged between steel and concrete according to their distributions. Both contributions are considered by the homogenized law. The rheological scheme of the model is presented on Figure 2.1. The homogenized stress is evaluated by combination of steel and concrete contributions, with the consideration of direction and quantity of reinforcement compared to concrete. Behaviour of reinforcements is modelled through an elasto-plastic law with a possible positive hardening. In each direction, stress is calculated and then multiplied by the reinforcement quantity before contributing to the homogenized law.

Concerning concrete contribution, it is evaluated in a poromechanical framework. The total stress is divided in two parts, the part which is applied on the solid skeleton $\widetilde{\sigma_{ij}}'$, and the other part acting on the interstitial phase P_i, weighted by Biot's coefficient b_i depending on the volume of the interstitial phase considered (ASR gels, DEF products, water), as presented in (1) :

$$\widetilde{\sigma_{ij}} = \widetilde{\sigma_{ij}}' - \sum b_i P_i \quad (1)$$

By this poromechanical formulation, the model can differentiate and link the macro and micro scales. Cracks induced by structural loads, are supposed to be localised, unlike those induced by internal poral pressure which are considered as diffuse. This distinction is made by plastic criteria which differ with the kind of loading. For structural effect, shear and compression are managed by an isotropic Drucker-

Prager criterion, for the tension it is by an anisotropic associated Rankine criterion. A same kind of criterion is also used to characterize plasticity induced by ASR pressure at pore scale.
In both scales, crack formation usually causes a reduction of mechanical performances. To consider such phenomenon, the model is based on damage theory. Thus, the model uses effective stress $\widetilde{\sigma_{kl}}$ which is linked to the total stress σ_{ij} in the constitutive equations, as presented in (2), in which D_{ijkl} is the anisotropic damage driven by plastic strains

$$\sigma_{ij} = (\delta_{ij}\delta_{kl} - D_{ijkl})\widetilde{\sigma_{kl}} \quad (2)$$

The model can evaluate different kinds of damage like those induced by external loading (tension, compression) but also internal phenomena (creep, shrinkage…).

As the present paper focuses on ASR evaluation with this chemo-mechanical approach, only these parts of the model are explained here. The other mechanical aspects of the model are already published in [3] and detailed in [1].

2.2 ASR model

2.2.1 Chemical advancement

Thermo-hydric conditions have important impacts on the ASR evolution. Temperature drives mostly the expansion kinetics [6] in a nonlinear way. In ASR, water is both the diffusion medium and a reactant: water content impacts both expansion range and advancement. In order to simulate such impact, and inspired by Poyet's works [7], this advancement A^{RAG} is limited by the saturation ratio Sr of concrete. The advancement law writes as:

$$\frac{\partial A^{RAG}}{\partial t} = \frac{1}{\tau_{ref}^{RAG}} C^{T,RAG} \cdot C^{W,RAG} \cdot \langle Sr - A^{RAG} \rangle_{+} \quad (3)$$

The temperature impact is modelled by a thermal activation coefficient $C^{T,RAG}$ driven by an Arrhenius law proposed by Larive [6] and implemented by Grimal [8]:

$$C^{T,RAG} = exp\left(-\frac{E^{RAG}}{R}\left(\frac{1}{T} - \frac{1}{T_{ref}}\right)\right) \quad (4)$$

With E^{RAG} the activation energy (estimated around 40 000J/Mol by Larive [6]), T_{ref}, the absolute reference temperature and τ_{ref}^{RAG}, the ASR characteristic time at T_{ref}.

The hydric activation coefficient $C^{W,RAG}$ was based on Poyet's work. Its has evolved toward a square form in Morenon's work [4] to obtain a greater impact at high saturation degree:

$$C^{W,RAG} = \begin{cases} \left(\dfrac{S_r - {S_r}^{th,RAG}}{1 - {S_r}^{th,RAG}}\right)^2 & if\ S_r > {S_r}^{th,RAG} \\ 0 & if\ S_r \leq {S_r}^{th,RAG} \end{cases} \quad (5)$$

Finally, the volume of ASR-gel induced by the reaction is obtained by multiplying this advancement by another material parameter which corresponds to the potential maximum quantity of gel $\Phi^{RAG,\infty}$. ASR-expansion occurs in three periods: latency time, expansion acceleration and asymptotic expansion. In a physical point of view, it is important to note the link between the reaction site consideration and the latency time. Bažant et Steffens [9], consider the reactive site at the paste/aggregate interface, justifying this time by the necessary time to fill the accessible surrounding porosity by the ASR-gel. Idorn [10] assumes the reactive sites are in the aggregate. With this consideration, the internal pressure rises until the cracking of the aggregate. Ichikawa and Miura [11] also consider the aggregate as reactive site, but conversely to other authors, they define the initial ASR-gel as a fluid. Once the calcium consumption is started, authors postulate a reaction rim formation. Once it formed, this reaction rim acts like a membrane which develops internal pressure with the ASR gel production. So even if the reason are still discussed in literature, two main mechanisms can explain the latency time: physical reasons (permeation of gels [9]) and / or chemical reasons (reaction rim formation

[11]). In the present work, the two mechanisms have been considered: a part of ASR-gels is supposed to form the reaction rim without participating to pressure and another part permeates through the porosity connected to reactive sites. The effective volume of gel Φ_g^{eff} which participates to pressure is defined with the A_{LAT}:

$$\Phi_g^{eff} = \Phi^{RAG,\infty} \frac{(A^{RAG}(t) - A_{LAT})}{(1 - A_{LAT})} \tag{6}$$

The reaction rim is supposed to be formed once $A^{RAG}(t) > A_{LAT}$.

2.2.2 ASR-pressure

The formation of ASR-products leads to internal pressure all around reactive sites. A part of this gel fills some accessible volume before inducing expansion. This volume is composed by the porosity connected to the reactive sites, Φ_g^v. The part of ASR-products which can permeate through this connected porosity becomes higher as the internal pressure increases. The elastic and delayed strains $(\varepsilon^{el} + \varepsilon^{cr})$ induce the modifications of the porosity in which ASR-products are formed and the volume induced by cracking $(\varepsilon^{p,ASR})$ can be filled by a part of the new products. Therefore, the pressure induced by ASR-products P_{ASR} must consider these dependences through the following equation:

$$P_{ASR} = M_{ASR} \left\langle \Phi_g^{eff} - \left\langle \Phi_g^v \left(\frac{P_{ASR}}{\widetilde{R_I^t}} \right) + b_{ASR} \cdot tr(\varepsilon^{el} + \varepsilon^{cr}) + (1 - b_{ASR}) tr(\varepsilon^{p,ASR}) \right\rangle^+ \right\rangle^+ \tag{7}$$

The Biot coefficient b_{ASR} and modulus M_{ASR} are used to consider the gel's rigidity and its interaction with the concrete matrix according to the poromechanical theory (1).Their values are fixed and defined as input data. In [12], Morenon proposed a calibration of b_{ASR} lying between 0.1 and 0.25. Concerning M_{ASR}, it is evaluated according to the Biot theory [13], considering the gel and matrix bulk modulus. Hence, the values used in this study are respectively 0.15 and 20,000 MPa.

2.2.3 Cracking and damage

The formation of ASR-products in concrete leads to internal pressure and thus to tensile stresses. If the tensile stress reaches the local tensile strength of concrete, cracking occurs. To evaluate the cracking induced by this internal pressure, an associated Rankine plastic criterion written in the poromechanical framework is used:

$$f_I^{ASR} = \tilde{\sigma}_I^{\,eq} - \widetilde{R_I^t} \;\; whith \;\; I \in [I, II, III] \qquad With \;\; \tilde{\sigma}_I^{\,eq} = P_{ASR} C^{ASR} + \min(\tilde{\sigma}_I, 0) \tag{8}$$

With C^{ASR} the stress concentration factor, P_{ASR} the internal pressure, $\tilde{\sigma}_I$ the effective stress and $\widetilde{R_I^t}$ the effective tensile strength. This mechanical strength has a hardening ability: greater stress is necessary to propagate more and more micro cracks. With this criterion, it is necessary to have a bigger external stress than the internal state to crack the matrix.

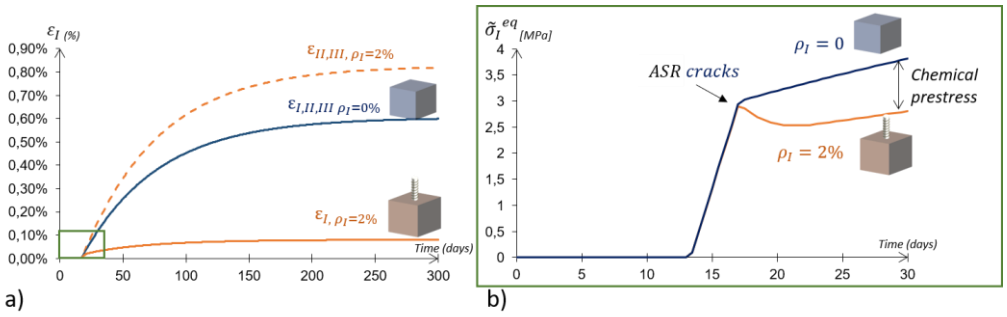

Figure 2.2: (a) Stress impact on swelling, (b) Effective stress in matrix and chemical prestress

The concrete swelling is allowed by the development of internal pressure induced by the ASR gel. If this pressure exceeds $\widetilde{R_I^t}$, corresponding to the local tensile strength, crack is initiated. If one direction is restrained as in [4] [5] [14] [15] or reinforced, chemical prestress is induced in the reinforcement. Figure 2.2 presents the numerical response of the model in the case of a ratio of reinforcement of 2% in a concrete submitted to a stress-free expansion of about 0.6%. The effective stress induced by the internal pressure is lower than in the case of stress- free expansion. This effective stress must reach the tensile strength before cracks appear perpendicular to the reinforcements. Cracking in the perpendicular direction of reinforcement is delayed but remains possible if expansion becomes sufficiently high [16].
The damage induced by ASR-expansion is calculated from the plastic strains derived from previous criteria used in each principal direction of stresses:

$$D_I^{t,ASR} = \frac{\varepsilon_I^{pl,ASR}}{\varepsilon_I^{pl,ASR} + \varepsilon^{k,ASR}} \tag{9}$$

$\varepsilon^{k,ASR}$ is a characteristic strain, equal to 0.3% for ASR [17].
As cracking induced by ASR can be reclosed by further compression, the material is less damaged by this kind of load. This effect is considered in the model by the ASR damage compressive law:

$$D_I^{c,ASR} = 1 - \left(\left(1 - D_{II}^{t,ASR}\right)\left(1 - D_{III}^{t,ASR}\right)\right)^{\alpha_{ASR}} \tag{10}$$

With α_{ASR} a coupling coefficient equal to 0.15, which weights the tensile damage tensor.
Note that these mechanical equations ((7), (8), (9), (10)) can be used for all the issues of over pressure in porosity like ASR but also like delayed ettringite formation. In fact, even if the chemical equations are different, the mechanical considerations present similar consequences [18]. The mechanical part of the model was validated by Morenon [12] on beams subjected to a moderate and an important swelling, and on two dams. Note that one of the beams, and one of the dams were submitted to delayed etringite formation (DEF).

2.3 Homogenized reinforcement model

2.3.1 Homogenized law

Once the damage induced by ASR in concrete is evaluated, the reinforcement contribution is calculated by the homogenized constitutive law.

Each reinforcement is defined by its direction, noted $\overrightarrow{Vr}$, with r corresponding to the reinforcement reference, and by its amount defined as a reinforcement ratio ρ^r (cross-section ratio of the reinforcement divided by the concrete cross-section) in the direction $\overrightarrow{Vr}$. Each finite element can have three directions of reinforcement (Figure 2.3). The constitutive law of the steel reinforcement is elasto-plastic.

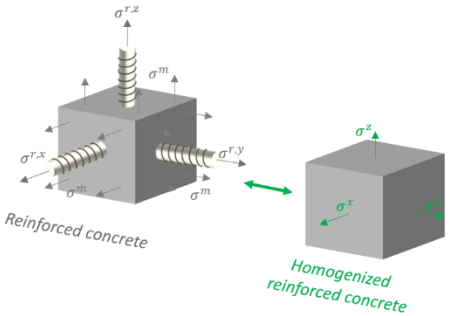

Figure 2.3: Homogenized reinforced concrete element

The homogenized constitutive law can be written as:

$$\sigma_{ij} = \left(1 - \sum_{n=1}^{Nr} \rho^n\right)\sigma_{ij}^m + \sum_{n=1}^{Nr} \rho^n \sigma_{ij}^{rn} \tag{11}$$

With Nr, the total number of reinforcing bars.

If a crack occurs in a reinforced finite element, and if its normal is different from those of reinforcement, the steel contribution in crack is considered. The reinforcement sees its direction evolved in or next to the crack and develop a contribution into this damaged zone. This phenomenon is called the dowel effect.

Evaluation of cracks is based on damage theory, and because a localized crack and an undamaged zone can develop into a same finite element, the steel participation must be considered in the two zones. Consequently, and according to the damage theory, total stress is evaluated with the stress contribution in the damage zone multiplied by the corresponding value of damage, and the part in undamaged zone multiplied by one minus this value. For more explanations on the dowel effect see [1].

2.3.2 Axial stress in reinforcement

In each reinforced direction $(\overrightarrow{Vr})$, the axial stress σ^r is evaluated by equation (12):

$$\sigma^r = E^r(\varepsilon^r - \varepsilon^{r,pl}) \tag{12}$$

With E^r the steel Young's modulus and $\varepsilon^r, \varepsilon^{r,pl}$ its total and plastic strains.

The plasticity is described by a uniaxial plastic criterion driven by a linear kinetic hardening:

$$f^r = |\sigma^r - H^r\varepsilon^{r,pl}| - f_y^r \tag{13}$$

With H^r the hardening modulus and f_y^r the elastic limit of the reinforcment.

This part of the model was validated by Chhun [19] on a strongly reinforced beam without ASR, and then used on a nuclear power plant containment wall during the operational phases but also in a loss of coolant accident (LOCA) scenario without ASR too.

3. CASE STUDY

3.1 Characteristics

3.1.1 Geometry

The modelling is based on experimental data from Ohno et al. [5]. They investigated the impact of ASR deterioration on concrete mechanical characteristics of reinforced beams. Two reinforced beams were casted: two reference non-reactive beams and two reactive beams. After an aging period, the beams were submitted to a four-point bending test until failure. Four 25 mm-diameter bars were embedded for the longitudinal reinforcement and 10 mm-diameter bars were used for transversal reinforcement (Figure 3.1).

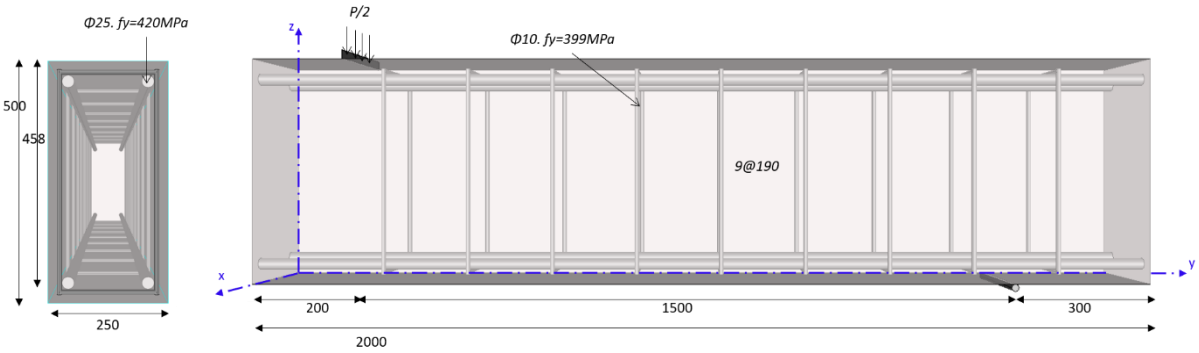

Figure 3.1: Half-beam reinforcement (unit mm)

The homogenized approach and even more generally the modelling, need beforehand to establish a mesh strategy depending on desired outcome. In the present study, it was decided to choose an element longitudinal size small enough to obtain a clear crack pattern. Because of small size of the transversal length, and because of the absence of significant effect in this direction, one element was enough for the transversal direction. For the vertical direction, the mesh depends on the calculation strategy and on the precision targeted for the crack pattern during the four-point bending test. For the longitudinal direction, the mean position of reinforcements must be respected. The definition of the zones of

homogenisation of the reinforcement depends on the type of loading. To obtain a correct flexural behaviour, the effective position of reinforcement must be correctly represented.

In this study, the longitudinal reinforcing steel were concentrated in the upper and lower chords. The centre of the area concerned must correspond to the centre of gravity of this reinforcement. It is illustrated in Figure 3.2 on the red part. For the transversal direction, the upper and lower horizontal parts of the reinforcement are concentrated in these elements too. Finally, due to limited effect in this direction and to limit the number of mesh elements, the vertical part of the transversal reinforcement could be homogenized over all the beam. The ratio is calculated with respect to the cross-section chosen for the reinforcement concentration. This distribution is shown on Figure 3.2.

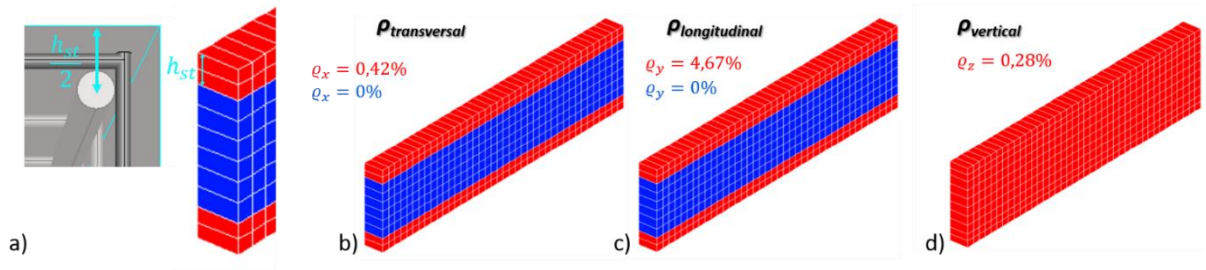

Figure 3.2: a) Steel height determination, b) Transversal steel ratio, c) Longitudinal steel ratio, d) Vertical steel ratio

Due to geometrical symmetries, only a quarter of the beam needs to be modelled. Displacements perpendicular to two faces are blocked to represent the symmetry conditions, in the longitudinal and transversal directions.

To simulate the simple support of the beam, only a line of the lower chord is blocked in the vertical direction. Similarly, the load is modelled by a displacement applied on a line of the upper fibre. These boundary conditions and specific lines are presented in Figure 3.3.

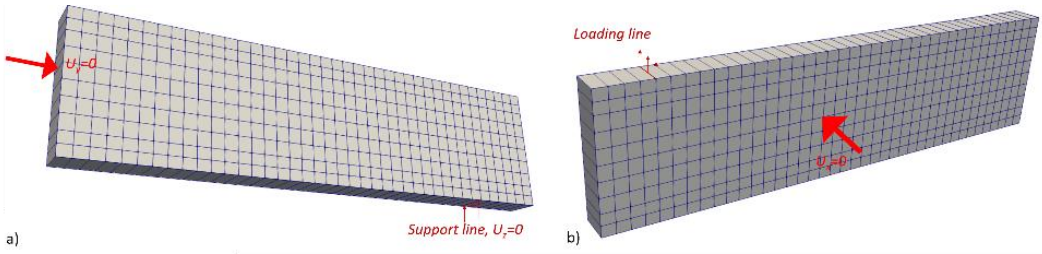

Figure 3.3: Boundary conditions a) Front view, b) Back view

In terms of environmental conditions, the beams were submitted to natural weather. The average temperatures per month during the 1984-1987 years are available and applied as an external boundary condition during the aging phase.

3.1.2 Study parameters

Young's modulus and compressive strength were evaluated by the authors at 28 days, 17 months and 45 months, these data are given and detailed in [5].

The evolution of concrete properties due to cement hydration is not considered in this numerical study. To obtain realistic evaluations the mechanical characteristics for the non-reactive beam chosen for the modelling are those corresponding to 17 months (the date of flexural tests). To highlight the chemical prestress and the structural effects induced by ASR compared to the non-reactive beams, it was decided to take the same mechanical characteristics for the reactive beams than for the non-reactive ones. Elastic modulus and compressive strength were respectively 27.5 MPa and 37 GPa. The tensile strength is then extrapolated from the compressive strength value from Eurocode 2 (NF_EN_1992).

For the reinforcement, yield strengths are given for the 25 mm diameter bar and for the 10 mm diameter bar, respectively 420 MPa and 399 MPa. The Young's modulus and hardening modulus have been assumed to take usual values: respectively 200,000 MPa and 1,000 MPa.

3.2 Aging of concrete

This experimental campaign was divided in two phases. First, an aging period of concrete was studied during which evolution of strains mainly due to temperature variations and ASR was monitored. The second part studied the beam response when submitted to a four-point bending test until failure. Two periods of aging were chosen to evaluate the flexural performance after different ASR advancements: seventeen months and forty-five months after concrete casting.

3.2.1 Monitoring and results

During the experiment, strains were measured by monitoring points along the beams. Six strains were monitored along the longitudinal direction and eight along the vertical direction. The gauge lengths were respectively 100 milimeters and 300 milimeters. The vertical position of the longitudinal monitoring points corresponded to the location of reinforcements. As this information is relative to the whole beam and as the model concerned only the half beam, half of these monitoring points are chosen and used. Hence, for the numerical evaluations, strains in four points are chosen for the longitudinal and vertical direction (at mid span, only the half longitudinal gauge length is used).

Displacements are recorded on each point and divided by the corresponding gauge length. These points and length are shown on the top of the Figure 3.4. The strategy of modelling consists to find first the correct ASR-parameters to simulate the expansion on reinforced concrete with time. For this calibration phase, a coarse mesh is first used until these parameters are well-evaluated. Once this calibration is obtained, the aging phase can be modelled with the real mesh. Strains are evaluated for the reactive and the non-reactive beams, in the control points. They are shown in comparison with the experimental value in Figure 3.4. The differences in strain of the non-reactive beam between numerical and experimental studies can be explained by local differences in temperature between the laboratory and the meteorological station. However, the range of thermal strains seems to be well-captured. The expansions in the two directions of the reactive beams are evaluated from the calibration of four parameters to evaluate the kinetics and the amplitude of ASR-expansion. The values of the calibrated input data are presented in Table 3.*1*. The results are obtained without modification of the hardening law for ASR-expansion calibrated in [4]. The effect of restraint of ASR due to reinforcement steels is thus well-reproduced. This is an important first result for this numerical study. The hardening law proposed in Morenon's work gives a correct representation of the anisotropic expansions in the reinforced beam compared to the experimental one, with a slight overestimation of the longitudinal strains.

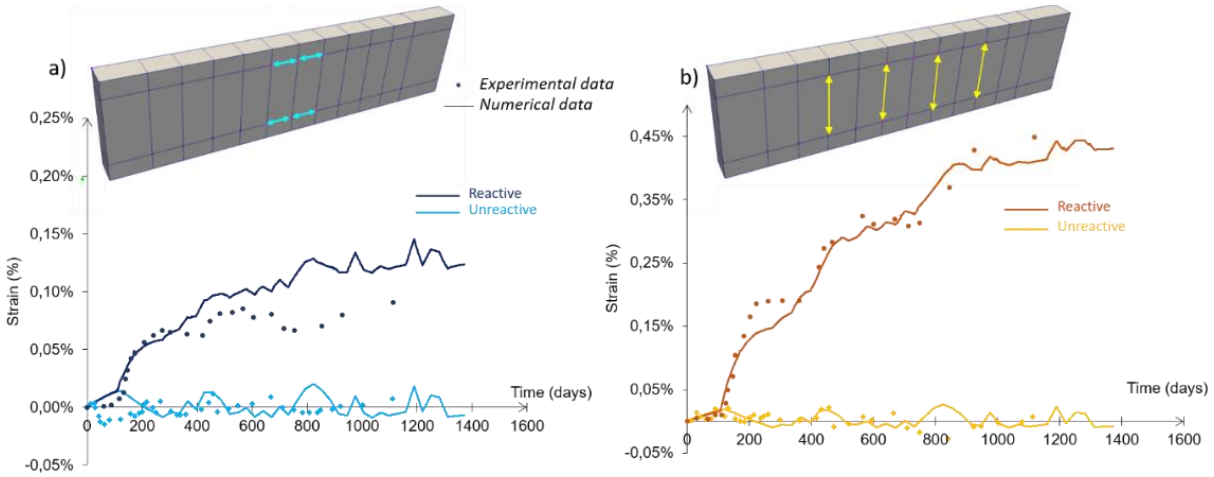

Figure 3.4: Strains evolution, a) Longitudinal direction, b) Vertical direction

Table 3.1: ASR input data values

	Corresponding equation	Value
τ_{ref}^{ASR}	(3)	*60 days*
$\Phi^{ASR,\infty}$	(6)	*0.021* m^3/m^3
A_{LAT}	(6)	*0.2* -
Φ_{ASR}^{v}	(7)	*0.0011* m^3/m^3

3.3 Four-point bending test

After the aging period, beams were submitted to a four-point bending test up to failure. The experience has thus been modelled in two stages. After the first one which corresponds to the aging phase, the calculus ended, and the beams are deformed by the first loading (thermal loading and ASR expansions). Thus, the loading line is in a final position different from the initial one. Those displacements are noted and then subtracted by a value of 14mm, corresponding to the average end-shift of the experimental load-displacement curves. In the second part of the modelling, this displacement evolution is imposed on the same line to model the flexural load. To avoid concrete creep phenomenon during this test, load is applied over 0.2 days. At the end of the load, the vertical displacement at the mid span line and the nodal forces at the load line were noted to establish the load-deflection curves.

The two types of beams (reactive and non-reactive) present similar experimental load-deflection curves at 17 months and at 45 months. But significant differences in the response can be observed between the reactive and non-reactive beams. These differences are induced by the structural effects of ASR on reinforced structures and have to be well-reproduced by the numerical responses of the model.

The experimental curves showed a lower initial rigidity for the reactive beams, due to the microcracking induced by the swelling. After the first tensile cracks due to flexion in non-reactive beams, this trend reverses and the reactive beams present the highest rigidity. More, rigidity of non-reactive beams decreased suddenly after the first flexural cracks, while the rigidity of reactive beams decreased more smoothly: due to chemical prestress, the first tensile cracks due to flexure appear for higher load in reactive beams [20]. The steel yielding appears for a smaller displacement for the reactive beams than for the non-reactive beams. The curves obtained by the modelling exhibit the same features, even if the numerical results predict a slightly too small rigidity for the reactive beams.

The differences in the response of the beams at different ages, as obtained by the modelling are small during the first part of the flexural test: the reactive beam tested after 45 months shows a rigidity slightly higher than the beam tested after 17 months before 175 kN. The small increase of rigidity is due to chemical prestress induced by ASR, which is more advanced in the case of the longest aging period (45 months). At the final stage, there is a small impact of this difference on the tensile stress at failure (around 6 MPa).

Finally, the ultimate values of these load/displacement curves are almost the same for all the beams. ASR seems not to induce significant differences on the ultimate flexural capacity, but mainly on its evolution as already described in the literature [5]. The important point for the numerical analysis is the capability of homogenized reinforced concrete modelling to reproduce these mechanical responses for all various cases.

Longitudinal stresses in reinforcement and in concrete are given in Figure 3.5 for the nonreactive and the reactive beams after the aging period of 45 months.

The comparison of the stresses in the reactive and nonreactive beams before the loading allows the chemical prestressing to be evaluated. In the reactive beam, the longitudinal reinforcements are already loaded in tension due to ASR at the end of the aging period, leading to partly confining concrete. The numerical analysis gives compressive stresses in the concrete of the reactive beams for 17 and 45 months of aging period respectively around 3 MPa and 3.8 MPa (0 MPa for the nonreactive).

When applying the flexural load, this confinement effect tends to limit the evolution of tensile phenomenon of the reactive beam. In the same way, due to the ASR and its tensile effect on reinforcement, the compressive evolution of the upper chords is more limited in the reactive upper chord than the non-reactive one.

The initial value of the unreactive case corresponds almost perfectly with experimental data. After the first crack of unreactive beam, the model appears to slightly overestimate the decrease of its initial rigidity induced by this local craking. For the reactive ones, this overestimate starts at the beginning of

the load evolution. Because of the use of the same Young's modulus for both cases, it seems to be due to a slight overestimation of the ASR induced tensile damage before loading.

The cracking patterns observed during experimentations at the end of the flexural tests for the reactive and the nonreactive beams are presented on the top of Figure 3.6. The dotted lines represent diffuse cracking induced by ASR, and plain lines indicate the cracks due to the flexural tests. Due to chemical prestress, shear cracks were less numerous for the reactive beams than for the nonreactive beams.

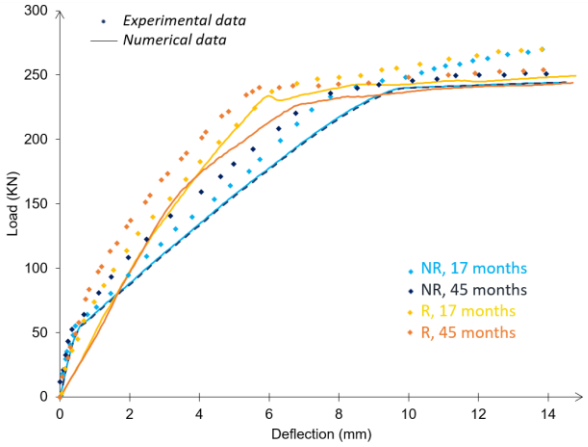

Figure 3.5: Load displacement curves

This specific difference between cracks patterns has been reproduced by the model (Figure 3.6). The presented maps show the maximal cracks openings along the three orthogonal directions for the non-reactive case (a)), the 17 months reactive case (b)) and the 45 months reactive one (c)). The number of cracks and their orientation along the beams are quite well-reproduced by the modelling. Particularly, the reactive beam exhibits less shear cracks than non-reactive beam as observed during the experimentations. The numerical calculations of the nonreactive beam show a large zone of diffuse cracks in the vertical direction rather than three or four localized cracks as observed in the reality. For the reactive cases, the beam tested after 45 months shows two flexural cracks at the end of the loading test while the beam tested after 17 months presents only one crack for the numerical analysis (only one pattern is given in [5] without precision on the date). Maximal crack opening are 1.3 mm and 0.7 mm for the beams at 17 months and 45 months, respectively. The difference can be explained by the slight difference in rigidity seen in the reactive load/displacement curves. The small and short rigidity overtaking of the 45 months case compared to the 17 months case can explain those results.

The beam tested after 45 months of aging period presents two main flexural cracks against only one main crack for the beam tested after 17 months, but the opening of the crack is greater for the beam tested after 17 months. Such evolution in resulting cracks is due to the modification of the stress state between the two ageing periods. After 45 months, the compressive stress due to restraint and the damage induced by ASR in the concrete are greater. The chemical prestressing and its consequences have an important effect on the final crack patterns.

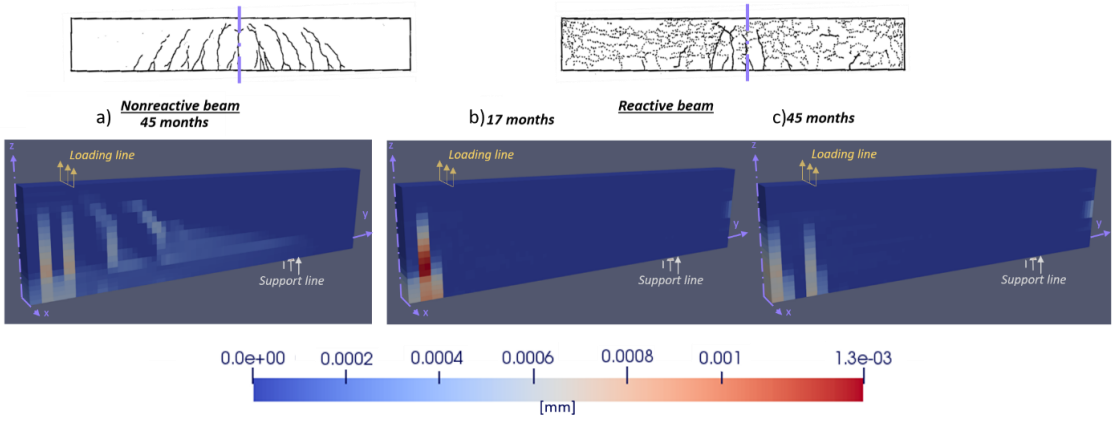

Figure 3.6: Experimental and modelling crack patterns of the a) Non-reactive beam, b) 17 months reactive beam, c) 45 months reactive beam

The responses of reinforced concrete beams, both reactive and non-reactive, have been well modelled. Despite a slight underestimation of the flexural rigidity compared to reality, the computed difference induced by the chemical prestress between the reactive and the nonreactive beams appears as realistic. Thus, homogenized model and its use are here validated in ASR-context for slender structures in environmental conditions. The following step will be to use this approach on massive structures damaged by ASR to evaluate the capacity of homogenised reinforcement to predict their structural behaviour. In this analysis, the anchorage conditions seem to be preserved during all the tests. A second part of the validation of the approach of homogenised reinforced concrete should concern the reinforcement slip issue to know how to manage such problem in structures.

4. CONCLUSION

The aim of this study was to validate the use of homogenized reinforced concrete model to predict the mechanical response of the reinforced concrete beams submitted to ASR. Anisotropic criterion and hardening law for ASR-expansion are needed to faithfully reproduce the experimental results of these tests, and particularly the chemical prestress induced by the expansion restraint and the different crack patterns of reactive and nonreactive beams.

First, numerical characteristics have been calibrated to reproduce the experimental swelling of beams, then the load/displacement curves have been well simulated without supplementary model modification. A slight flexural rigidity underestimation was founded in the modelling. This effect may be due to two imprecisions: the choice of the initial mechanical characteristics from the experimental data or the use of a too severe plastic criterion.

The use of the homogenized method allows bypassing limitations induced by the reinforcement meshing like loss of bond which generally leads to a loss of mechanical strength. The modelled load-displacement curves show the absence of this kind of issue in this case and validate the interest of this method. To complete this process of validation, the model needs to be evaluated in other kinds of structure.

5. ACKNOWLEDGEMENTS

Dr S. Ohno and Dr. Y. Kawabata are thanked for important precisions on test conditions.

Acknowledgement is addressed to Electricité de France (EDF) for its financial support on the EXIGENCE project which is the framework of the present study. The modelling was made with the finite element software developed by EDF R&D, Code_Aster (V14.2, https://www.code-aster.org) and the post-processing with Salome_Meca.

6. REFERENCES

[1] Sellier A. Anisotropic Damage and Visco-Elasto-Plasticity Applied to Multiphasic Materials. [Research Report] LMDC - Laboratoire Matériaux et Durabilité des Constructions de Toulouse ; Université de Toulouse III - Paul Sabatier; INSA de Toulouse. 2018. https://hal.insa-toulouse.fr/hal-01710289v2/document

[2] Pietruszczak S, Winnicki A. Constitutive Model for Concrete with Embedded Sets of Reinforcement. Journal of Engineering Mechanics-ASCE 2003;129. https://doi.org/10.1061/(ASCE)0733-9399(2003)129:7(725).

[3] Sellier A, Millard A. A homogenized formulation to account for sliding of non-meshed reinforcements during the cracking of brittle matrix composites: Application to reinforced concrete. Engineering Fracture Mechanics 2019;213:182–96. https://doi.org/10.1016/j.engfracmech.2019.04.008.

[4] Morenon P, Multon S, Sellier A, Grimal E, Hamon F, Bourdarot E. Impact of stresses and restraints on ASR expansion. Construction and Building Materials 2017;140:58–74. https://doi.org/10.1016/j.conbuildmat.2017.02.067.

[5] Ohno S, Yoshioka Y, Shinozaki Y, Morikawa T. The mechanical behaviour of reinforced beams coated after Alkali-Silica Reaction damage. 8th international conference on Alkali-aggregate reaction. Kyoto, Japan, 1989, p. 697–702.

[6] Larive C. Apports combinés de l'expérimentation et de la modelisation à la compréhension de l'alcali-reaction et de ses effets mécaniques. PhD Thesis. École nationale des ponts et chaussées (France), 1998.

[7] Poyet S. Study of Alkali-Silica Reaction affected concrete structures: experimental approach and multi-scale numerical simulations in a variable hydro-chemo-mechanical environment. Theses. Université de Marne la Vallée, 2003.

[8] Grimal E. Caractérisation des effets du gonflement provoqué par la réaction alcali-silice sur le comportement mécanique d'une structure en béton. PhD Thesis. Université de Toulouse, Université Toulouse III-Paul Sabatier, 2007.

[9] Bazant ZP. Microplane model for strain-controlled inelastic behaviour. In: Desai CS, Gallagher RH, editors. Mechanics of Engineering Materials, John Wiley & Sons; 1984, p. 45–59.

[10] M. Idorn G. A discussion of the paper "Mathematical model for kinetics of alkali–silica reaction in concrete" by Zdenek P. Bazant and Alexander Steffens. Cement and Concrete Research 2001;31:1109–10. https://doi.org/10.1016/S0008-8846(01)00522-1.

[11] Ichikawa T, Miura M. Modified model of alkali-silica reaction. Cement and Concrete Research 2007;37:1291–7. https://doi.org/10.1016/j.cemconres.2007.06.008.

[12] Morenon P. Modélisation des réactions de gonflement interne des bétons avec prise en compte des couplages poro-mécaniques et chimiques. PhD Thesis. Université de Toulouse, Université Toulouse III-Paul Sabatier, 2017.

[13] Biot MA. General theory of three-dimensional consolidation. Journal of Applied Physics 1941;12:155–164.

[14] Jones AEK. Cracking, expansion and strength of concrete subjected to restrained alkali silica reaction. PhD Thesis. University of Birmingham, 1994.

[15] Muranaka M, Tanaka Y. Development of Physical and Chemical Model for Concrete Expansion Due to Asr Based on Reaction Mechanism. Journal of Japan Society of Civil Engineers, Ser E2 (Materials and Concrete Structures) 2013;69:1–15. https://doi.org/10.2208/jscejmcs.69.1.

[16] Kagimoto H, Yasuda Y, Kawamura M. ASR expansion, expansive pressure and cracking in concrete prisms under various degrees of restraint. Cement and Concrete Research 2014;59:1–15. https://doi.org/10.1016/j.cemconres.2014.01.018.

[17] Capra B, Sellier A. Orthotropic modelling of alkali-aggregate reaction in concrete structures: numerical simulations. Mechanics of Materials 2003;35:817–30. https://doi.org/10.1016/S0167-6636(02)00209-0.

[18] Multon S, Sellier A. Expansion modelling based on cracking induced by the formation of new phases in concrete. International Journal of Solids and Structures 2019;160:293–306. https://doi.org/10.1016/j.ijsolstr.2018.11.001.

[19] Chhun P. Modélisation du comportement thermo-hydro-chemo-mécanique des enceintes de confinement nucléaire en béton armé-précontraint. PhD Thesis. Université de Toulouse, Université Toulouse III-Paul Sabatier, 2017.

[20] Morenon P, Multon S, Sellier A, Grimal E, Hamon F, Kolmayer P. Flexural performance of reinforced concrete beams damaged by Alkali-Silica Reaction. Cement and Concrete Composites 2019;104:103412. https://doi.org/10.1016/j.cemconcomp.2019.103412.